Encoding of Tactile Context in the Mouse Visual Cortex

Steffen Kandler,[1,2,7] Dun Mao,[1,3,7] Bruce L. McNaughton,[1,3,4] and Vincent Bonin[1,5,6,8,*]

[1]Neuro-Electronics Research Flanders (NERF), Kapeldreef 75, 3001 Leuven, Belgium

[2]Imec, Kapeldreef 75, 3001 Leuven, Belgium

[3]Canadian Centre for Behavioral Neuroscience (CCBN), University of Lethbridge, Lethbridge, Alberta T1K 3M4, Canada

[4]Department of Neurobiology and Behavior, University of California Irvine, USA

[5]Vlaams Instituut voor Biotechnologie (VIB), 3001 Leuven, Belgium

[6]Department of Biology, KU Leuven, Naamsestraat 61, 3000 Leuven, Belgium

[7]These authors contributed equally

[8]Lead Contact

*Correspondence: vincent.bonin@nerf.be

SUMMARY

Primary sensory cortices have been linked to the processing and perception of signals from non-preferred sensory modalities. The cellular activity patterns underlying these cross-modal influences, however, are not known and measurements in intact animals during ethologically relevant behaviours are lacking. We examined the hypothesis that, during real-world behaviour, tactile inputs are encoded in the rodent primary visual cortex (V1) enabling the contextualisation of visual signals. We studied cellular activity in mouse V1 during active exploration of a controlled tactile environment. We identified a population of V1 neurons that specifically encodes tactile stimuli sensed by the whiskers. The neurons show activation in response to tactile stimuli independent of visual inputs. The responses are diverse and selective providing diverse contextual and locational information. In addition, V1 visually responsive cells show response modulations linked to tactile stimuli suggesting they receive subthreshold inputs from tactile neurons. These results indicate that mouse V1 encodes functionally diverse cross-modal signals during real-world behaviour. They suggest a coding strategy whereby signals from distant brain regions converge onto functionally distinct cell groups in primary sensory areas to mediate contextual modulations of primary sensory activity. This convergence may enable early multisensory associations in aid of navigation or exploration behaviours.

Keywords

Visual cortex; Tactile activity; Cross-modal; Calcium imaging; Two-photon

Highlights

- Head-fixed exploration assay to study influence of tactile context on V1 processing.
- V1 subpopulation preferentially encodes somatosensory inputs from the whiskers.
- V1 tactile responses carry diverse contextual and locational information.
- V1 visual responses show modulations linked to tactile inputs.

In Brief

By imaging mouse V1 neurons during head-fixed exploration of a controlled tactile environment, Kandler et al. show that V1 neurons exhibit diverse cross-modal contextual activity modulations and identify a cell subpopulation that preferentially encodes somatosensory inputs from the whiskers.

INTRODUCTION

There is a growing body of data linking primary sensory cortices to multisensory processing (Driver and Noesselt, 2008; Ghazanfar and Schroeder, 2006; Schroeder and Foxe, 2005; Stein and Stanford, 2008). The primary visual cortex (V1) receives abundant multimodal projections from other sensory cortical areas (Charbonneau et al., 2012; Falchier et al., 2002; Kim et al., 2015; Masse et al., 2016; Rockland and Ojima, 2003; Stehberg et al., 2014; Van Brussel et al., 2011). EEG recordings and functional imaging studies show that V1 is subject to cross-modal influences of its neural activity at the level of aggregate neural ensembles (De Meo et al., 2015; Murray et al., 2015). Similar effects are observed in blind and sighted subjects (Amedi et al., 2010; Merabet and Pascual-Leone, 2010; Sathian, 2005) suggesting a role for this activity in normal sensory function.

In vivo physiological studies in monkeys and rodents also indicate influences of cross-modal stimuli on the activity of individual V1 neurons. Cross-modal stimulation can produce subthreshold inputs and modulate neuronal outputs (Bieler et al., 2017; Ibrahim et al., 2016; Iurilli et al., 2012; Kayser et al., 2008, 2009; Lakatos et al., 2009; Wang et al., 2008) and even

activate cortical neurons (Bieler et al., 2017; Bizley et al., 2007; Ibrahim et al., 2016; Newton et al., 2002; Wallace et al., 2004). Activation of a specific neuronal population by auditory stimulation has been reported (Ibrahim et al., 2016). However, there is little data on the tuning of cross-modal signals in V1 and other primary sensory cortices.

Animals make use of visual and somatosensory information to move through their environment. Vision and touch provide distinct yet complementary information about objects (Kleinfeld et al., 2006), obstacles (Sofroniew et al., 2014), and self-motion (Jenks et al., 2010). Studies in humans and monkeys have shown that V1 can respond to tactile stimuli and is involved in tactile perception (Guipponi et al., 2015; Murray et al., 2015; Pascual-Leone et al., 2005; Sathian and Zangaladze, 2002; Zangaladze et al., 1999). Studies in rodents show that passive mechanical stimulation of the whiskers can hyperpolarize V1 membrane potentials and suppress neural firing (Iurilli et al., 2012). While tactile stimuli provide subthreshold inputs whether they can activate V1 neurons is debated (Bieler et al., 2017; Newton et al., 2002; Vasconcelos et al., 2011; Wallace et al., 2004). Studies in freely-moving rats, however, reported activity linked to location (Haggerty and Ji, 2015 1508; Ji and Wilson, 2007), objects and tactile behaviour (Vasconcelos et al., 2011), which could reflect tactile inputs. Precisely what tactile information is encoded in V1 during behaviour is unclear and how signals from preferred and non-preferred sensory modalities are encoded in V1 populations is not well understood.

We investigated the impact of tactile inputs on activity in the mouse primary visual cortex during head-fixed active whisking and locomotor behaviour using controlled sensory stimuli. We identified a population of neurons that show specific responses to tactile stimuli encoding somatosensory inputs from the whiskers. These neurons showed diversely tuned responses to stimuli and location in the tactile environment. Visual responsive cells showed response modulations that could be traced back to tactile stimuli in the environment. These results indicate that mouse V1 encodes functionally diverse cross-modal signals during navigation or exploration behaviours. This convergence of cross-modal information onto a functionally distinct cell group may enable early multisensory associations in aid of ethological relevant behaviours.

RESULTS

To investigate the encoding of tactile information in the mouse primary visual cortex (V1), we combined cellular imaging with a head-fixed treadmill locomotion assay. C57Bl/6j mice (n = 23 animals) were implanted with a head fixation plate and trained to voluntarily run on a low-friction 150-cm linear treadmill for a water reward (Fig. 1A; Suppl. Figs S1A–C, S2). After 2-3 weeks of training (typ. 10 to 15 sessions), the animals were highly engaged during the task (Suppl. Fig. S1D), running at high speed (typ. 20 cm/s, range 10 to 50 cm/s) for sessions lasting 1 hour, generating hundreds of laps per session.

To probe the neurons' sensory response properties, animals were head-fixed under a two-photon microscope and visual and tactile stimuli were delivered as animals ran on the treadmill (Fig. 1A; Suppl. Fig. S1A–C,G). Somatic calcium signals were imaged from GCaMP6-labeled neurons in V1 layer 2/3 (125 to 350 μm below pia) through a glass window implanted over left posterior cortex. Sensory stimuli were delivered upon treadmill movement. For visual stimulation, pseudo-random stimuli were shown to the contralateral right eye as the animal ran across fixed locations on the treadmill (see Experimental Procedures). For tactile stimulation, strips of material attached to the treadmill belt surface were used to periodically contact the whiskers as the animals moved the belt (Suppl. Fig. S1H; Suppl. Figs S2B). A shield positioned just above the treadmill blocked the belt and approaching tactile stimuli from the animal's line of sight (Fig. 1A; Suppl. Fig. S1A-B). Taking movement speed into account, each strip was within the whiskers' reach for only a few tens of milliseconds. Cellular imaging in the S1 barrel field of the somatosensory cortex confirmed robust responses from somatosensory neurons (Suppl. Fig. S3C). To examine the responses, calcium time courses were deconvolved and expressed as a function of location on the treadmill in 1-cm intervals, normalizing activity by time spent at individual intervals (Gothard et al., 1996; Mao et al.). Only activity during locomotion epochs (> 2 cm/s) was considered. The resulting position related activity profiles allowed relating the neurons' firing responses to tactile stimuli on the treadmill (Suppl. Fig. S3D).

Activation of V1 Neurons by Tactile Stimuli

To determine whether V1 neurons show somatosensory responses to tactile stimuli during locomotion on the treadmill, we compared activity in darkness and at a photopic light level on treadmills with or without stimuli (Fig. 1B; Suppl. Fig. S2B). Animals were trained on a treadmill

devoid of stimuli (blank belt, Suppl. Fig. S2A). Activity from the same population of neurons was measured in consecutive blocks of trials on a treadmill devoid of stimuli and on a treadmill with two identical sets of stimuli (Fig. 1B,C; see Experimental Procedures, Experiment 1). To test for inputs from the whiskers or the paws, we measured, in a separate block of trials, V1 activity on a treadmill with tactile stimuli in presence of a barrier preventing whiskers from touching the belt and stimuli (Fig. 1B).

We obtained the calcium activity courses of 2,925 layer 2/3 neurons from monocular V1 (n = 7 mice). For all experiments, the two-photon microscope was centred on the retinotopic subregion of V1 activated by a monocular visual stimulus of 60 deg. width centred at 45 deg. azimuth and 0 deg. elevation. We focused our analyses on neurons that showed one or more calcium transients in at least 25 % of the laps (> baseline dF/F_0 + 3-times s.d.) (2,925 / 3,317 cells). To identify cells responding to the tactile stimuli, we compared calcium activity in a time window preceding the animals reaching the tactile stimuli to a similarly sized window centred on the stimuli. We identified cells that showed a pronounced increase in fluorescence at least at one of the tactile stimuli (1-way ANOVA, $p < 0.01$; > 10 % dF/F_0) and examined their activities in the blank belt and whisker barrier conditions.

About 9 % of the layer 2/3 neurons active during the task showed robust responses to the tactile stimuli (n = 112/1,270 cells) (Fig. 1C–F). As can be appreciated from the computed position related activity profiles (Fig. 1C, middle; Suppl. Fig. S5D, right), these cells showed a sharp increase in calcium fluorescence at the tactile stimuli but little indication of activation elsewhere. The responses were specific to the stimuli; no position-locked calcium transients were observed on the belt devoid of stimuli (Fig. 1C, left, Suppl. Fig. S5D, left). Consistent with responses encoding touches between the whiskers and the stimuli, no responses to the tactile stimuli were observed from these neurons in the barrier condition (Fig. 1C, right). Responses were abolished even though the animals' paws had full access to the stimuli and running behaviour maintained (Fig. 1C, bottom).

Across the population of neurons activated by tactile stimuli, the average response across trials was 16.1 ± 1.8 % dF/F_0 (mean ± s.e.m.). This is several-fold the activity at matched locations on the belt devoid of stimuli (1.1 ± 0.8 % dF/F_0, mean ± s.e.m.) (n = 112/1,270 cells) and in the

barrier condition (dF/F_0: 15.4 ± 3.1 % vs. 2.3 ± 1.1 %, mean ± s.e.m, $p < 1.5e\text{-}6$, paired sign test) (Fig. 1D,F). In presence of the barrier, responses were close to those observed on the blank belt (dF/F_0: $p < 0.1$; paired sign test) (Fig. 1F, 2B) and to those of the unresponsive population (Suppl. Fig. S5A). Importantly, these responses to tactile stimuli were observed both in darkness (< 0.01 cd/m^2) (n = 4 animals) and under photopic illumination (59 cd/m^2) (n = 7 animals). The fraction of activated neurons and the amplitudes of responses were similar across illumination conditions (Fig. 1D–F).

Somatosensory Inputs vs. Neuromodulatory Influences

These activity patterns were inconsistent with general neuromodulatory or motor influences. Activation by tactile stimuli was restricted to a small subset of neurons (Suppl. Fig. S5C). No calcium transients linked to tactile stimuli were observed in the remainder of the population (Suppl. Fig. S5D). Pronounced responses were observed in absence of concomitant changes in movement speed and pupil size (Fig. 1C, bottom; Suppl. Fig. S1E). Finally, both locomotion and tactile stimuli had little impact on pupil size (Suppl. Fig. S1F).

To directly examine the possibility that the activity reflects motor output, we related the activity to movement onsets and offsets (Suppl. Fig. S4). Neither pupil size nor locomotion onsets and offsets explained the calcium transients observed at the tactile stimuli (Suppl. Fig. S4). This excludes roles for arousal and motor influences in the observed responses to tactile stimuli.

Single Trial Responses to Tactile Stimuli

Responses to tactile stimuli were discernible in individual trials (Fig. 2). The amplitude of single trial calcium transients of neurons activated by tactile stimuli was 105.1 ± 66.5 % dF/F_0 (n = 1,345; > baseline dF/F_0 + 3-times s.d.). Transients of such magnitudes correspond to neurons firing multiple action potentials in V1 layer 2/3 (Chen et al., 2013). The responses to tactile stimuli occurred from the first trials the animals ran on the belt with stimuli (Fig. 2A,C,D). Responses were in fact observed in naïve animals that were never exposed to the belt with tactile stimuli (Fig. 2C). Responses showed no sign of abating as the animal ran multiple laps on the treadmill with stimuli (Fig. 2A,C,D) and disappeared from the first trials with the barrier (Fig. 2A, bottom).

194 **Consistency of Activity Across Trials**

195 Transient onsets were consistently aligned to the stimuli across trials (Fig. 2A,C,D; Suppl. Fig.
196 S4). The trial-to-trial alignment led to strong position related dependence seen in the average
197 activity (Fig. 1C; Suppl. S5D). To examine this dependency, calcium time courses were
198 deconvolved and expressed as a function of position. To quantify consistency of activity across
199 trials, we calculated the fraction of variance in the single-lap, data that is explained by the
200 average across laps (EV position; two-fold cross-validation, see Experimental Procedures).
201
202 On the belt with tactile stimuli, the average across laps explained 17.4 ± 1.3 % of the variance in
203 the deconvolved single trial data (mean ± s.e.m.; n = 112/1,270 cells). On the belt lacking tactile
204 stimuli, EV position was lower (4.5 ± 0.6 %) close to that observed in the broader population (EV
205 position: 5.1 ± 0.2 % vs. 3.1 ± 0.1 % mean ± s.e.m.) (n = 1158/1,270 cells). Similar results were
206 obtained in experiments with the barrier (EV position: 15.1 ± 2.0 % vs. 2.3 ± 0.3 %, mean ±
207 s.e.m., $p < 5.6e-8$, paired sign test) (n = 25/390 cells). In presence of the barrier, EV position
208 was close to that observed on the blank belt (dF/F_0: $p < 0.1$, EV position: $p < 0.42$; paired sign
209 test) (Fig. 1F, 2B) and that of the unresponsive population (Suppl. Fig. S5A). Amongst neurons
210 activated by tactile stimuli, EV position was similar in 'naïve' animals never exposed to a belt
211 with stimuli and previously-exposed animals (Fig. 2E).
212
213 **Tactile Stimuli Activate a Distinct Neural Population**
214 Do tactile activated neurons form a functionally distinct population? To determine whether
215 neurons activated by tactile stimuli respond to visual stimulation and vice versa, we measured
216 responses to tactile or visual stimuli from the same neural population (Fig. 3; Suppl. Figs S5,
217 S2C). For tactile stimulation, repeated strips of material were placed at two locations on the
218 treadmill belt. For visual stimulation, a brief, 1-sec visual stimulus was presented in lockstep
219 with locomotion as the animal ran across either of two treadmill locations. The responses to the
220 visual stimuli were assessed by comparing average calcium activities in 0.5-sec and 1.5-sec
221 windows before and after stimulus onsets. Responses to the tactile stimuli were assessed as
222 described above. Neurons were deemed responsive if activity was increased at either one of the
223 two stimulus locations (1-way ANOVA, $p < 0.01$).
224

We found no evidence of bimodal activation in the populations of layer 2/3 neurons we examined (Fig. 3A; Suppl. Fig. S5C–G) (n = 7 animals). Neurons activated by the tactile stimuli (n = 51/716 cells) showed no noticeable responses to the visual stimulus (Fig. 3A, cells 1,2; Suppl. Fig. S5F,G). Conversely, the neurons that showed activation by the visual stimulus (n = 97/716 cells) showed no responses to the tactile stimuli (Fig. 3A, cells 3,4; Suppl. Fig. S5F,G). The lack of bimodal activation is likely not a consequence of the neurons' low probability of activation. Assuming independent sampling, taking the number of responsive cells and sample size into account, the mean number of bimodal neurons expected is 6.9 ± 2.6 (mean ± s.d.) and the probability of no activation is less than one in one thousand ($p < 9.6e\text{-}4$). The lack of bimodal activation is likely not a consequence of the specific visual stimulus tested. Similar results were obtained in a separate group of mice using prolonged visual stimuli that covered a broad range of spatiotemporal frequencies and orientations (Suppl. Fig. S6) (n = 3 animals). Tactile neurons showed no activation to the broad range of visual stimuli (Suppl. Fig. S6B,D), providing further evidence of their functional distinct properties.

V1 Activity on the Treadmill with Diverse Stimuli

Cross-modal tactile activity could either be indiscriminate or tuned to specific tactile inputs encoding specific information about the stimuli in the tactile environment. To distinguish between these possibilities, we examined, in a separate group of animals (n = 4 mice), activity of layer 2/3 neurons while animals ran in a feature-rich tactile environment composed of strips of material of different heights and orientations placed at distinct treadmill locations (Fig. 4A; Suppl. Fig. S2D; see Experimental Procedures, Experiment 3). The 1-sec visual stimulus was presented as the animal ran across four distinct locations on the treadmill. No visual stimulus was presented during stationary epochs. To cast a wide net for cells that encode tactile information, we selected cells that showed repeated position-related activity patterns across trials (EV position > 10 %, two-fold cross-validation, see Experimental Procedures) (Fig. 4C) excluding cells that showed responses to the visual stimulus (EV visual stim. ≤ 0 %, two-fold cross-validation) (Figs 1–3). There was a general association between tactile stimuli on the belt and the number of V1 neurons that met these criteria (Fig. 4H). We therefore henceforth refer to these neurons as 'tactile' or 'putative tactile'.

To study the diversity of V1 tactile activity, we examined the calcium time courses of a total of 1,878 V1 layer 2/3 neurons (n = 4 animals) on the treadmill with diverse stimuli. We followed through on the 1,345 cells that showed calcium transients in over 25 % of laps (transients larger than baseline raw dF/F_0 + 3-times s.d.) excluding the remainder from further analysis. To examine the tuning of the activity, calcium time courses were deconvolved and expressed as a function of treadmill location, divided in 1-cm intervals.

About a quarter of active neurons (n = 353/1,345 cells) showed position-related responses (Fig. 4C, blue traces; EV position > 10 %, EV visual stim. ≤ 0 %, Fig. 4D,E) consistent with the activity of tactile neurons (Figs 1–3). This fraction of cells was on par with the fraction of cells entrained by the visual stimulus presented simultaneously as the animal ran on the treadmill with diverse stimuli (28 %, n = 378/1,345 cells, including responses locked to visual stimulus onset and offset) (Fig. 4B, red traces; EV visual stim. > 10 %) (Suppl. Fig. S7B,C). However, the fraction was two to several-fold larger than the fraction observed on treadmills with fewer tactile stimuli including the treadmill devoid of purposefully salient stimuli (Fig. 4H). These putative tactile neurons showed robust activity showing calcium transients of similar amplitudes as visually-responsive cells (tactile dF/F_0: 71.9 ± 61.4 %, visual dF/F_0: 69.8 ± 59.9.0 %, mean ± s.d.; transients larger than 3-times s.d. above baseline dF/F_0). The neurons showed similar activity levels during locomotion and stationary epochs (Fig. 4G). However, they were more active during stationary epochs than the visually-responsive cells (Fig. 4F, compare with Fig. 4G, no visual stimuli were presented during stationary epochs),

Far from indiscriminate, however, tactile activity was diversely tuned, with different neurons showing activity at specific locations in the tactile environment. Simultaneously imaged neurons showed distinct activity time courses (Fig. 4C, blue traces) and position-related activity patterns (Fig. 5A,B). Within a same imaging experiment, patterns with sharp and narrow-peak tuning to different locations were observed simultaneously with patterns showing more gradual activity changes with belt location. The patterns were repeatable. The average position-related activity across laps explained up to 50% of the variance in the single-trial data (EV position: 15.7 ± 10.9 %, mean ± s.d., two-fold cross-validation) (n = 353/1,345 cells) (Fig. 4E). The cross-correlation of activity across laps often showed a narrow peak of a few centimetres in width (8.2 ± 2.9 cm, half-width at half-maximum, mean ± s.d.) (Fig. 5C). Across the population, nonvisual neurons

showed location selectivity and position preferences that were distributed over the length of the treadmill belt (Fig. 5D).

While correlated with location, the activity of V1 tactile neurons did not bear the features of a place code (Suppl. Fig. S8). The activity of individual neurons showed considerable redundancy in time and space (Suppl. Fig. S8A,B). This high redundancy differs markedly from the sparse activity of hippocampal CA1 neurons measured during the same task (n = 3 animals) (Mao et al., 2017) (Suppl. Fig. S8C,D). During locomotion on the treadmill with diverse stimuli, hippocampal place cells showed low probability of activation (Suppl. Fig. S8C), sequential activation during movement (Suppl. Fig. S8C), and spatially-localized firing fields uniformly distributed over the treadmill (Suppl. Fig. S8D).

By comparison, V1 neurons showing tactile-like activity responded at multiple locations (Suppl. Fig. S8A,B) and showed no indication of sequential activation of V1 neurons during movement (Suppl. Fig. S8A). Furthermore, while robust hippocampal place cell activity was observed in absence of tactile stimuli (Suppl. Fig. S8E), the V1 neurons showed little spatial modulations of their activity on treadmills devoid of tactile stimuli (Fig. 4H). These properties are consistent with V1 neurons activity encoding low-level sensory features of the tactile environment.

We conclude that, rather than showing indiscriminate responses to tactile stimuli, V1 nonvisual neurons have diversely tuned response properties potentially encoding specific information about the tactile environment.

Modulations of Visual Responses by Tactile Context

Do tactile inputs sensed by the whiskers also influence V1 visual activity? While we found no indication of activation by tactile stimuli in visually-responsive cells (Figs 3–5), the neurons may receive subthreshold inputs that could influence responses to visual stimulation. To test for this possibility, we examined how responses to the repeated visual stimulus change as animals run across distinct sets of stimuli on the treadmill with diverse tactile stimuli (Fig. 6, same data as Figs 4,5). To study modulations across layers of V1, we complemented the layer 2/3 cellular imaging data (n = 4 + 3 mice) with acute single-unit electrophysiological recordings with multisite silicon probes in the same task (n = 5 animals).

Concomitant to the pronounced nonvisual activity (Figs 4C, 5B,C), V1 neurons showed marked trial-to-trial variability of visual responses during locomotion on the treadmill with diverse stimuli (Fig. 4B). In the cellular imaging data, variability was often not shared between simultaneously imaged neurons (Fig. 4B). In both cellular imaging data and acute recordings, variability was often linked to the location of visual stimulus onset (Fig. 6A; Suppl. Fig. S9A). To quantify these modulations, we sorted responses by treadmill location of stimulus onsets and averaged them across trials (Fig. 6A; Suppl. Fig. S9A). We focused on the three locations away from the reward site which had comparable pupil size, movement speed and eye position (Fig. 6B; Suppl. Fig. S9A). We computed for each cell a modulation index (MI) and effect size (ES), providing measures of the magnitude of the modulation and its difference in mean to the position-shuffled data (Suppl. Fig. S9B) (see Experimental Procedures). We excluded responses to the stimulus presented at the reward site which showed correlated eye movements and changes in movement speed (Suppl. Fig. S9A). Cellular imaging calcium time courses was deconvolved to estimate firing rates.

Although simultaneously imaged neurons responded, on average, similarly across the three locations (Fig. 6A, bottom), a subset showed pronounced and diverse activity differences across the three locations (Fig. 6A, cells 1 to 8). These differences were observed although pupil size and movement speed were similar at those locations (Fig. 6B; Suppl. Fig. S9A). Over two thirds of visually-responsive cells in layer 2/3 measured with cellular imaging showed clear location modulations (81 %, n = 306/378 cells in 4 animals, ES > 1) (Fig. 6E; Suppl. Fig. S9C). The neurons showed an average modulation index of 14.6 ± 13.9 % (mean ± s.d., n = 378 cells). Modulations by location were also observed in the electrophysiological recordings across layers, with two third of the cells showing modulations with an effect size > 1 (Fig. 6C; Suppl. Fig. S9D) (67 %, n = 98/146 cells in 5 animals, ES > 1). The average modulation index in the recordings across layers was 9.2 ± 7.3 % (mean ± s.d., n = 146 cells). Interestingly, modulations were observed at all depths of V1 (Fig. 6D).

To test whether modulations reflect behavioural variables correlated with location, we computed the Pearson correlation coefficient between the responses and behavioural variables over the time scale of the visual stimulus (Suppl. Fig. S9E,G). We considered movement speed (Suppl. Fig. S9E, top; S9G, left), interval between visual stimulus events (visual stimulation rate, Suppl.

Fig. S9E, middle; Suppl. Fig. S9G, right), and eye position (Suppl. Fig. S9E, bottom). The neurons' behavioural activity correlations were largely statistically independent from modulation indices, as evidenced by their separable joint histograms (Suppl. Fig. S9E,G). This held for electrophysiological recordings (Suppl. Fig. S9E) and the calcium imaging data (Suppl. Fig. S9E). One exception was movement speed, whereby highest correlated cells showed lower modulations. This was not observed in the spike recordings (Suppl. Fig. S9E, top). To test the impact of time spent at reward on modulations, we compared modulation indices across the slowest and fastest laps in the experiments measured around the reward site (bottom vs. top 25 % of trials) but found that it had weak impact on magnitude of modulations and effect size (Suppl. Fig. S9F). These results suggest that it is unlikely that location modulations of visual responses reflect correlations of behavioural variables with location.

To directly test the role of tactile stimuli on the belt, we imaged, in a separate group of animals (n = 3 mice), location modulation of visual responses in consecutive blocks of trials in presence of the barrier preventing access of the whiskers to tactile stimuli. Neurons showed weaker modulations in the presence of the barrier, with a mean modulation index of 19.1 ± 2.1 % (mean ± s.e.m., barrier placed, n = 83 cells) and 35.6 ± 4.6 % (mean ± s.e.m., barrier absent, $p < 9.0e-4$, 1-way ANOVA) and mean effect size of 1.5 ± 0.14 (mean ± s.e.m., barrier placed) and 2.3 ± 0.15 (barrier absent, $p < 3.0e-4$) (Fig. 6F).

Thus, during locomotion on the treadmill with diverse stimuli, V1 neurons show location-related modulations of visual responses that likely reflect tactile context.

DISCUSSION

We used a head-fixed active whisking and locomotion assay with controlled sensory stimuli to study contextual modulations by tactile inputs in the mouse primary visual cortex during behaviour. We found that during locomotion and exploration mouse V1 neurons encode rich information about tactile environment, encoding somatosensory inputs from the whiskers and partaking in visuo-tactile integration. These results indicate that mouse V1 encodes functionally diverse cross-modal signals during real-world behaviour.

We observed activation of mouse V1 layer 2/3 neurons by tactile stimuli (Figs 1–5) as well as modulations of visual responses by tactile context (Fig. 6). The tactile activity resembled the responses of neurons in the S1 barrel field of the somatosensory cortex (Suppl. Fig. S3), was observed both in darkness and under photopic illumination, and was disrupted by a barrier placed between the whiskers and the stimuli (Figs 1,2). Interestingly, the activity was carried by a cell population that show little responses to visual stimuli (Figs 3,4; Suppl. Fig. S6). This raises the interesting possibility that the neurons form a functionally distinct cell type. The responses were diverse and tuned to features and locations in the tactile environment (Figs 4,5).

Cross-Modal Activity in Primary Visual Cortex

Prior to this study, cellular level evidence of cross-modal activity in the rodent visual cortex stemmed primarily from electrical recordings of neuronal responses to passive stimulation (Bieler et al., 2017; Ibrahim et al., 2016; Iurilli et al., 2012; Newton et al., 2002; Wallace et al., 2004). These studies concluded that, in intact animals, cross-modal stimulation induces subthreshold inputs and modulates visual responses but seldom leads to neuronal activation without inputs from the primary sensory modality. A study of auditory stimulation (Ibrahim et al., 2016) reported activation of layer 1 inhibitory neurons but only modulations in layer 2/3 neurons. These studies used single or a few stimuli and could not address the degree to which V1 neurons encode diverse information about the cross-sensory modality. One study in freely moving rats (Vasconcelos et al., 2011) showed, in darkness, V1 activity linked to location and objects as well as modulations correlated with tactile discrimination behaviour. This study, however, could not distinguish between sensory or motor influences on V1 activity and did not investigate the tuning of individual V1 neurons.

A number of factors might have contributed to our observation of neuronal activation in response to tactile stimuli. First and foremost is the cellular imaging which has high yield and sensitivity and allows investigation of sparse firing patterns that could easily be overlooked with electrical recordings techniques. Our findings could be also influenced by the elevated excitability of V1 neurons during treadmill locomotion, which is associated with elevated arousal. However, a study in head-fixed mice reported similar subthreshold cross-modal responses to auditory stimulation during anaesthesia, wakefulness and movement (Iurilli et al., 2012). Accordingly, we observed similar levels of activity in tactile V1 neurons during locomotion and

stationary epochs (Fig. 4G). A third factor could be the active whisking paradigm. Somatosensory responses in S1 during active whisking are stronger and longer lasting than during passive stimulation (Krupa et al., 2004).

Function of V1 Tactile Signals

Our results indicate that diverse tactile signals are represented at the level of neuronal populations within mouse V1. The function of these signals remains to be elucidated. Convergence of complementary inputs from the eyes and the whiskers suggests integration of information from the animals' proximal tactile environment. This may be useful in exploratory or navigation behaviours such as object exploration (Vasconcelos et al., 2011) or obstacle avoidance (Sofroniew et al., 2014). While we observed no multimodal activity that would support multisensory associations, the modulations may serve contextualisation of visual inputs.

While correlated with location on the linear treadmill, the activity comprised the properties of a low-level sensory code. The activity was concentrated at the tactile stimuli (Figs 1–3, 5H) and had limited spatial selectivity (Fig. 5E, Suppl. Fig. S8A,B), with individual neurons responding at different times and showing responses at multiple locations during locomotion on the treadmill with diverse stimuli. This activity differs strikingly from the sparse and spatially localized activity we observed in hippocampus (Suppl. Fig. S8C,D) and in retrosplenial cortex (Mao et al., 2017) during the same task. We speculate that the diversity of the activity (Figs 4,5) reflects distinct whiskers brushing different tactile stimuli. Our experiments, however, do not rule out a contribution of stereotyped whisking patterns in generating the activity. Importantly, we note that position-related patterns provide only a lower bound on diversity and ignore the rich temporal dynamics of tactile activity (Suppl. Fig. S4). Understanding the precise whisker movements and touch patterns that lead to V1 tactile responses requires future investigation.

Origins of V1 Tactile Signals

The anatomical origins of V1 tactile signals are unknown. The activity could originate in long-range cortical inputs from S1 barrel field (Charbonneau et al., 2012; Kim et al., 2015; Masse et al., 2016; Stehberg et al., 2014; Van Brussel et al., 2011). Anterior visual cortical areas A and RL of the posterior parietal cortex are also interconnected with S1 barrel field (Wang et al., 2012). Neurons in area RL have been shown to respond to both visual and tactile stimulation

(Olcese et al., 2013). Neurons in these areas could send tactile information directly to V1 or relay tactile signals through any one of the higher visual cortical areas projecting to V1.

Relation to Cross-Modal Plasticity

There is a striking parallel between our results and the cross-modal plasticity that occurs in V1 following the loss of visual inputs (Amedi et al., 2010; Klinge et al., 2010; Lee and Whitt, 2015; Merabet et al., 2007; Sathian, 2005). Human neuroimaging studies have shown V1 activation in blind subjects during braille reading and other tactile paradigms (Merabet et al., 2007; Sadato et al., 1996). Cross-modal activity in V1 is also observed after short-term visual deprivation and is causally linked to tactile behaviour (Merabet et al., 2008; Merabet et al., 2007). In rodents, recovery of activity from loss of visual inputs depends on the inputs from the whiskers (Newton et al., 2002; Van Brussel et al., 2011). Following loss of visual inputs, the tactile activity we observe in intact animals may be amplified, which could explain the whisker-dependent, progressive recovery of activity in V1 that is observed weeks after removal of visual inputs.

SUPPLEMENTAL INFORMATION

Supplemental Information includes nine figures.

AUTHOR CONTRIBUTIONS

S.K., D.M., B.L.M and V.B. designed the experiments. D.M. and S.K. devised the behavioural assay. S.K. performed the experiments in the visual cortex. D.M. performed the dual recordings in cortex and hippocampus and the imaging in the hippocampus. S.K. and D.M. analysed the data with guidance from V.B. S.K. and V.B. wrote the manuscript with input from D.M. and B.L.M. The authors declare no competing interests.

ACKNOWLEDGEMENTS

We are grateful to Karel Svoboda, Judith Hirsch, Georg Keller, Thomas Mrsic-Flogel, Mark L. Andermann, Karl Farrow, Fabian Kloosterman, João Couto, Michał Ślęzak, and all members of the Bonin laboratory for feedback, discussions and comments on the manuscript. João Couto acquired the cellular imaging data set in the somatosensory cortex. Anna Pitas, Çağatay Aydın, and Xu Han assisted in experiments. Thanks to Molly J. Kirk and Alexandra Emmendorfer for

surgical help. We thank Adrienne Caiado, Jordyn Hanover, Jake T. Jordan, Jessica Mitchell, Frederique Ooms, Ben Puccio, and Daniel Tovbin for animal training. We thank Adrian Cheng for technical advice with the two-photon microscopes. This work was supported by Neuro-Electronics Research Flanders (B.L.M. and V.B.), AIHS Polaris award (B.L.M.), AIHS graduate studentship (D.M.), NSERC funding (B.L.M.), NSF grant 1631465 (B.L.M.), Research Foundation—Flanders (FWO) grant G0D0516N (V.B.), and KU Leuven Research Council grant C14/16/048 (V.B.).

REFERENCES

Amedi, A., Raz, N., Azulay, H., Malach, R., and Zohary, E. (2010). Cortical activity during tactile exploration of objects in blind and sighted humans. Restor Neurol Neurosci *28*, 143-156.

Bieler, M., Sieben, K., Schildt, S., Roder, B., and Hanganu-Opatz, I.L. (2017). Visual-tactile processing in primary somatosensory cortex emerges before cross-modal experience. Synapse *71*.

Bizley, J.K., Nodal, F.R., Bajo, V.M., Nelken, I., and King, A.J. (2007). Physiological and anatomical evidence for multisensory interactions in auditory cortex. Cereb Cortex *17*, 2172-2189.

Bonin, V., Histed, M.H., Yurgenson, S., and Reid, R.C. (2011). Local diversity and fine-scale organization of receptive fields in mouse visual cortex. J Neurosci *31*, 18506-18521.

Charbonneau, V., Laramee, M.E., Boucher, V., Bronchti, G., and Boire, D. (2012). Cortical and subcortical projections to primary visual cortex in anophthalmic, enucleated and sighted mice. Eur J Neurosci *36*, 2949-2963.

Chen, T.W., Wardill, T.J., Sun, Y., Pulver, S.R., Renninger, S.L., Baohan, A., Schreiter, E.R., Kerr, R.A., Orger, M.B., Jayaraman, V.*, et al.* (2013). Ultrasensitive fluorescent proteins for imaging neuronal activity. Nature *499*, 295-300.

Dana, H., Chen, T.W., Hu, A., Shields, B.C., Guo, C., Looger, L.L., Kim, D.S., and Svoboda, K. (2014). Thy1-GCaMP6 transgenic mice for neuronal population imaging in vivo. PLoS ONE *9*, e108697.

De Meo, R., Murray, M.M., Clarke, S., and Matusz, P.J. (2015). Top-down control and early multisensory processes: chicken vs. egg. Front Integr Neurosci *9*, 17.

Driver, J., and Noesselt, T. (2008). Multisensory interplay reveals crossmodal influences on 'sensory-specific' brain regions, neural responses, and judgments. Neuron *57*, 11-23.

Falchier, A., Clavagnier, S., Barone, P., and Kennedy, H. (2002). Anatomical evidence of multimodal integration in primate striate cortex. J Neurosci *22*, 5749-5759.

Ghazanfar, A.A., and Schroeder, C.E. (2006). Is neocortex essentially multisensory? Trends in cognitive sciences *10*, 278-285.

Goldey, G.J., Roumis, D.K., Glickfeld, L.L., Kerlin, A.M., Reid, R.C., Bonin, V., Schafer, D.P., and Andermann, M.L. (2014). Removable cranial windows for long-term imaging in awake mice. Nat Protoc *9*, 2515-2538.

Gothard, K.M., Skaggs, W.E., and McNaughton, B.L. (1996). Dynamics of mismatch correction in the hippocampal ensemble code for space: interaction between path integration and environmental cues. J Neurosci *16*, 8027-8040.

Guipponi, O., Clery, J., Odouard, S., Wardak, C., and Ben Hamed, S. (2015). Whole brain mapping of visual and tactile convergence in the macaque monkey. Neuroimage *117*, 93-102.

Haggerty, D.C., and Ji, D. (2015). Activities of visual cortical and hippocampal neurons co-fluctuate in freely moving rats during spatial behavior. Elife *4*.

Hazan, L., Zugaro, M., and Buzsaki, G. (2006). Klusters, NeuroScope, NDManager: a free software suite for neurophysiological data processing and visualization. J Neurosci Methods *155*, 207-216.

Ibrahim, L.A., Mesik, L., Ji, X.Y., Fang, Q., Li, H.F., Li, Y.T., Zingg, B., Zhang, L.I., and Tao, H.W. (2016). Cross-Modality Sharpening of Visual Cortical Processing through Layer-1-Mediated Inhibition and Disinhibition. Neuron *89*, 1031-1045.

Iurilli, G., Ghezzi, D., Olcese, U., Lassi, G., Nazzaro, C., Tonini, R., Tucci, V., Benfenati, F., and Medini, P. (2012). Sound-driven synaptic inhibition in primary visual cortex. Neuron *73*, 814-828.

Jenks, R.A., Vaziri, A., Boloori, A.R., and Stanley, G.B. (2010). Self-motion and the shaping of sensory signals. J Neurophysiol *103*, 2195-2207.

Ji, D., and Wilson, M.A. (2007). Coordinated memory replay in the visual cortex and hippocampus during sleep. Nat Neurosci *10*, 100-107.

Kadir, S.N., Goodman, D.F., and Harris, K.D. (2014). High-dimensional cluster analysis with the masked EM algorithm. Neural Comput *26*, 2379-2394.

Kayser, C., Petkov, C.I., and Logothetis, N.K. (2008). Visual modulation of neurons in auditory cortex. Cereb Cortex *18*, 1560-1574.

Kayser, C., Petkov, C.I., and Logothetis, N.K. (2009). Multisensory interactions in primate auditory cortex: fMRI and electrophysiology. Hear Res *258*, 80-88.

Kim, E.J., Juavinett, A.L., Kyubwa, E.M., Jacobs, M.W., and Callaway, E.M. (2015). Three Types of Cortical Layer 5 Neurons That Differ in Brain-wide Connectivity and Function. Neuron *88*, 1253-1267.

Kleinfeld, D., Ahissar, E., and Diamond, M.E. (2006). Active sensation: insights from the rodent vibrissa sensorimotor system. Curr Opin Neurobiol *16*, 435-444.

Klinge, C., Eippert, F., Roder, B., and Buchel, C. (2010). Corticocortical connections mediate primary visual cortex responses to auditory stimulation in the blind. J Neurosci *30*, 12798-12805.

Krupa, D.J., Wiest, M.C., Shuler, M.G., Laubach, M., and Nicolelis, M.A. (2004). Layer-specific somatosensory cortical activation during active tactile discrimination. Science *304*, 1989-1992.

Lakatos, P., O'Connell, M.N., Barczak, A., Mills, A., Javitt, D.C., and Schroeder, C.E. (2009). The leading sense: supramodal control of neurophysiological context by attention. Neuron *64*, 419-430.

Lee, H.K., and Whitt, J.L. (2015). Cross-modal synaptic plasticity in adult primary sensory cortices. Curr Opin Neurobiol *35*, 119-126.

Mao, D., Kandler, S., McNaughton, B.L., and Bonin, V. (2017). Sparse orthogonal population representation of spatial context in the retrosplenial cortex. Nat Commun *8*, 243.

Masse, I.O., Ross, S., Bronchti, G., and Boire, D. (2016). Asymmetric Direct Reciprocal Connections Between Primary Visual and Somatosensory Cortices of the Mouse. Cereb Cortex.

Merabet, L.B., Hamilton, R., Schlaug, G., Swisher, J.D., Kiriakopoulos, E.T., Pitskel, N.B., Kauffman, T., and Pascual-Leone, A. (2008). Rapid and reversible recruitment of early visual cortex for touch. PLoS ONE *3*, e3046.

Merabet, L.B., and Pascual-Leone, A. (2010). Neural reorganization following sensory loss: the opportunity of change. Nat Rev Neurosci *11*, 44-52.

563 Merabet, L.B., Swisher, J.D., McMains, S.A., Halko, M.A., Amedi, A., Pascual-Leone, A., and Somers,
564 D.C. (2007). Combined activation and deactivation of visual cortex during tactile sensory
565 processing. J Neurophysiol *97*, 1633-1641.

566 Murray, M.M., Thelen, A., Thut, G., Romei, V., Martuzzi, R., and Matusz, P.J. (2015). The multisensory
567 function of the human primary visual cortex. Neuropsychologia.

568 Newton, J.R., Sikes, R.W., and Skavenski, A.A. (2002). Cross-modal plasticity after monocular
569 enucleation of the adult rabbit. Exp Brain Res *144*, 423-429.

570 Niell, C.M., and Stryker, M.P. (2008). Highly selective receptive fields in mouse visual cortex. J Neurosci
571 *28*, 7520-7536.

572 Olcese, U., Iurilli, G., and Medini, P. (2013). Cellular and synaptic architecture of multisensory integration
573 in the mouse neocortex. Neuron *79*, 579-593.

574 Pascual-Leone, A., Amedi, A., Fregni, F., and Merabet, L.B. (2005). The plastic human brain cortex. Annu
575 Rev Neurosci *28*, 377-401.

576 Rockland, K.S., and Ojima, H. (2003). Multisensory convergence in calcarine visual areas in macaque
577 monkey. Int J Psychophysiol *50*, 19-26.

578 Royer, S., Zemelman, B.V., Losonczy, A., Kim, J., Chance, F., Magee, J.C., and Buzsaki, G. (2012).
579 Control of timing, rate and bursts of hippocampal place cells by dendritic and somatic inhibition.
580 Nat Neurosci *15*, 769-775.

581 Sadato, N., Pascual-Leone, A., Grafman, J., Ibanez, V., Deiber, M.P., Dold, G., and Hallett, M. (1996).
582 Activation of the primary visual cortex by Braille reading in blind subjects. Nature *380*, 526-528.

583 Sathian, K. (2005). Visual cortical activity during tactile perception in the sighted and the visually
584 deprived. Dev Psychobiol *46*, 279-286.

585 Sathian, K., and Zangaladze, A. (2002). Feeling with the mind's eye: contribution of visual cortex to tactile
586 perception. Behav Brain Res *135*, 127-132.

587 Schroeder, C.E., and Foxe, J. (2005). Multisensory contributions to low-level, 'unisensory' processing.
588 Curr Opin Neurobiol *15*, 454-458.

589 Smith, S.L., and Hausser, M. (2010). Parallel processing of visual space by neighboring neurons in
590 mouse visual cortex. Nat Neurosci *13*, 1144-1149.

591 Sofroniew, N.J., Cohen, J.D., Lee, A.K., and Svoboda, K. (2014). Natural whisker-guided behavior by
592 head-fixed mice in tactile virtual reality. J Neurosci *34*, 9537-9550.

593 Stehberg, J., Dang, P.T., and Frostig, R.D. (2014). Unimodal primary sensory cortices are directly
594 connected by long-range horizontal projections in the rat sensory cortex. Front Neuroanat *8*, 93.

595 Stein, B.E., and Stanford, T.R. (2008). Multisensory integration: current issues from the perspective of the
596 single neuron. Nat Rev Neurosci *9*, 255-266.

597 Terrazas, A., Krause, M., Lipa, P., Gothard, K.M., Barnes, C.A., and McNaughton, B.L. (2005). Self-
598 motion and the hippocampal spatial metric. J Neurosci *25*, 8085-8096.

599 Thevenaz, P., Ruttimann, U.E., and Unser, M. (1998). A pyramid approach to subpixel registration based
600 on intensity. IEEE Trans Image Process *7*, 27-41.

601 Van Brussel, L., Gerits, A., and Arckens, L. (2011). Evidence for cross-modal plasticity in adult mouse
602 visual cortex following monocular enucleation. Cereb Cortex *21*, 2133-2146.

603 Vasconcelos, N., Pantoja, J., Belchior, H., Caixeta, F.V., Faber, J., Freire, M.A., Cota, V.R., Anibal de
604 Macedo, E., Laplagne, D.A., Gomes, H.M.*, et al.* (2011). Cross-modal responses in the primary
605 visual cortex encode complex objects and correlate with tactile discrimination. Proc Natl Acad
606 Sci U S A *108*, 15408-15413.

607 Vogelstein, J.T., Packer, A.M., Machado, T.A., Sippy, T., Babadi, B., Yuste, R., and Paninski, L. (2010).
608 Fast nonnegative deconvolution for spike train inference from population calcium imaging. J
609 Neurophys *104*, 3691-3704.

610 Wallace, M.T., Ramachandran, R., and Stein, B.E. (2004). A revised view of sensory cortical parcellation.
611 Proc Natl Acad Sci U S A *101*, 2167-2172.

612 Wang, Q., and Burkhalter, A. (2007). Area map of mouse visual cortex. J Comp Neurol *502*, 339-357.

613 Wang, Q., Sporns, O., and Burkhalter, A. (2012). Network analysis of corticocortical connections reveals
614 ventral and dorsal processing streams in mouse visual cortex. J Neurosci *32*, 4386-4399.

615 Wang, Y., Celebrini, S., Trotter, Y., and Barone, P. (2008). Visuo-auditory interactions in the primary
616 visual cortex of the behaving monkey: electrophysiological evidence. BMC Neurosci *9*, 79.

617 Zangaladze, A., Epstein, C.M., Grafton, S.T., and Sathian, K. (1999). Involvement of visual cortex in
618 tactile discrimination of orientation. Nature *401*, 587-590.

619

FIGURE LEGENDS

Figure 1. V1 Neurons Show Whisker-Related Responses to Tactile Stimuli

(A) Assay to study multisensory activity in primary visual cortex (V1) of awake mice. Mice run head-fixed on a 150-cm treadmill while tactile stimuli (blue) are delivered to the whiskers and visual stimuli (red) to the contralateral eye. A water reward is delivered at the end of each lap. Cellular activity is measured in monocular V1 layer 2/3 using a two-photon microscope. A shield (black) blocks the approaching tactile stimuli from eyesight. Treadmill position, movement speed, eye position and pupil size are monitored. Bottom: A removable barrier placed between the animals' snout and treadmill belt prevents the whiskers from contacting tactile stimuli. Bottom right: GCaMP6 labelled neurons in superficial V1 imaged through a cranial window (scale bar, 20 μm). See also Suppl. Figs S1A–C, S2, S3.

(B) Experiment to identify tactile responsive V1 neurons. Top to bottom: Experiments consist of three blocks of trials: First, mice run on a belt without tactile stimuli. Subsequently, the belt is replaced with one containing tactile stimuli (blue, T1,T2), while head-fixation and the microscope field-of-view are maintained. Tactile stimuli comprise two discrete 10-cm stretches of four thin, 5-mm wide foam strips. Finally, whisker contacts with the stimuli are blocked with a removable whisker barrier (orange). Experiments are performed without visual stimuli in darkness. See also Suppl. Figs S1H, S2B.

(C) Trial average calcium fluorescence as a function of treadmill position of two simultaneously imaged V1 L2/3 neurons. These neurons show sharp calcium increases at tactile stimuli locations (centre, blue) but not in the no-stimulus condition (left). The whisker barrier disrupts tactile activity (right, yellow) Top: Illustration of treadmill belts. Shaded areas indicate treadmill position of tactile stimuli. Shaded curves represent s.e.m. computed across trials. Locomotion behaviour shown below (mean ± s.d.; blank: n=69 laps, tactile: n=76 laps, barrier: n=58 laps). Activity is measured without visual inputs and in darkness (< 0.01 cd/m^2).

(D) Normalized calcium activity of 25 cells with significant responses at tactile stimuli location (1-way ANOVA, $p < 0.01$) in presence and absence of tactile stimuli. Tactile responses are largely disrupted by the whisker barrier. Experiments are done in darkness (< 0.01 cd/m^2).

(E) Normalized activity of 112 cells with responses at tactile stimuli location (1-way ANOVA, $p < 0.01$) in presence and absence of stimuli. Experiments are done under photopic condition (grey screen illumination). See also Suppl. Fig. S2B.

652 (F) Cumulative distributions of responses for tactile responsive cells in the three experimental
653 conditions (no. stim., tactile stim. and barrier) in darkness (solid curves) and in the two
654 conditions (no stim. and tactile stim.) in photopic conditions (dashed curves). See also Suppl.
655 Fig. S5A.
656

Figure 1.

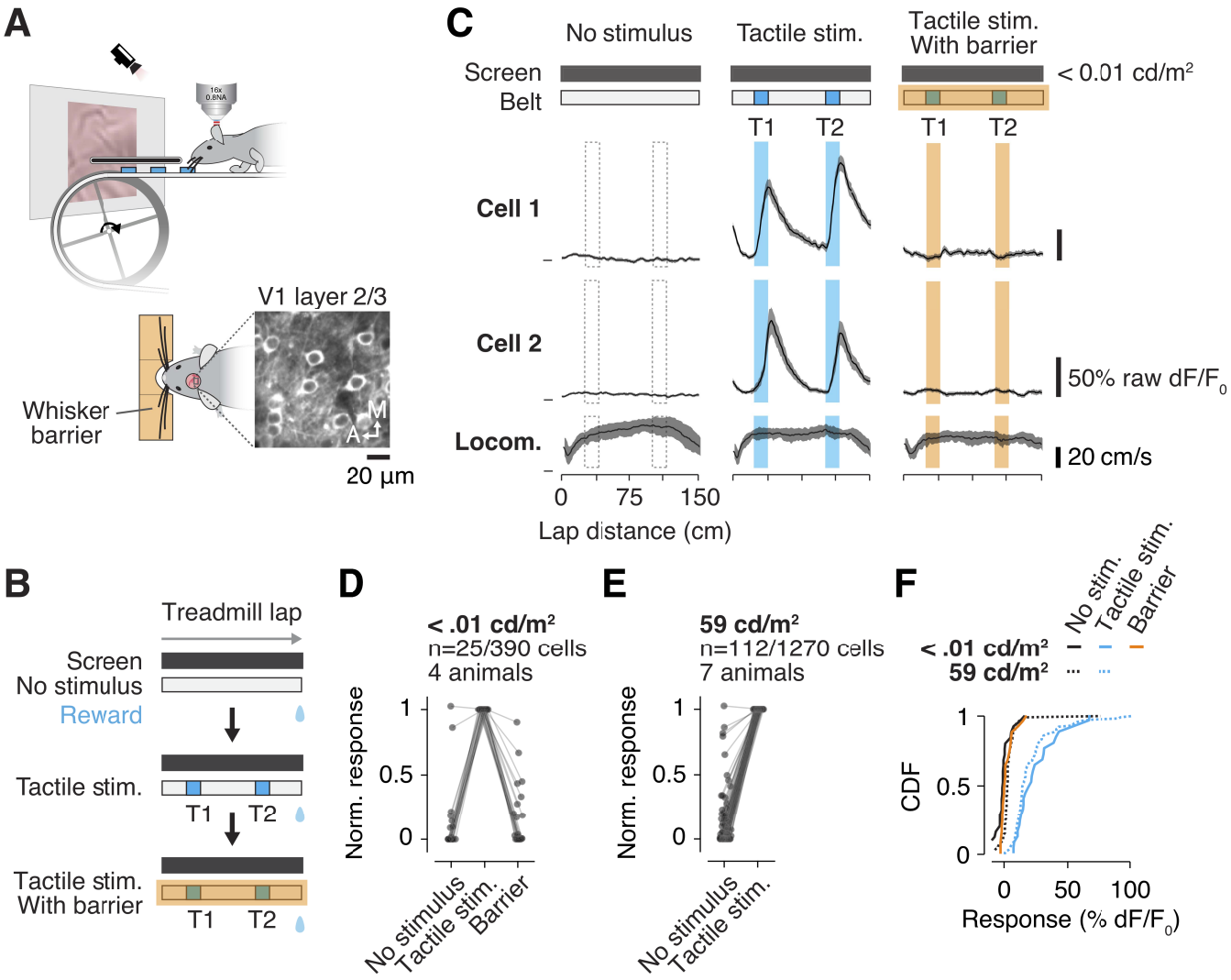

Figure 2. Prior Exposure Is Not Required for V1 Tactile Activity

(A) Trial-to-trial activity of two neurons with and without tactile stimuli and with the whisker barrier. Top: Block of trials on the treadmill without tactile stimuli. Centre: Block of trials with stimuli, without the barrier. Bottom: Block of trials with the barrier preventing contacts between whiskers and tactile stimuli. Note how tactile responses are observed from the first laps on the treadmill with tactile stimuli (centre) and how they are abolished from the first laps with the barrier (bottom). For visualization, a subset of the laps is omitted for the no-stimulus condition. See also Suppl. Fig. S4A.

(B) Population quantification of entrainment of activity of cells by tactile stimuli in presence and absence of the whisker barrier. Note the activity entrainment without stimuli and in presence of the whisker barrier matches the unresponsive population.

(C) Trial-to-trial activity of two V1 neurons in an animal that was never exposed to a treadmill with tactile stimuli. Top: Block of trials on treadmill without stimuli. Bottom: Block of trials on treadmill with tactile stimuli. Note how tactile responses are observed from the first laps on the treadmill with stimuli and how tactile neurons can show haphazard ongoing activity in absence of tactile stimuli. See also Suppl. Fig. S4B.

(D) Trial-to-trial activity of two V1 neurons from an animal with prior experience on a treadmill with tactile stimuli. Note the lack of activity in absence of tactile stimuli despite prior exposure to the stimuli. For visualization, a subset of the laps is omitted for the no-stimulus condition. See also Suppl. Fig. S4C.

(E) Cumulative distributions of tactile responding cells for the two experimental conditions (no stim. and tactile stim.) in naïve (dashed curves) and experienced (solid curves) animals for their responses (left) and entrainment of activity (right). See also Suppl. Fig. S5B.

Figure 2.

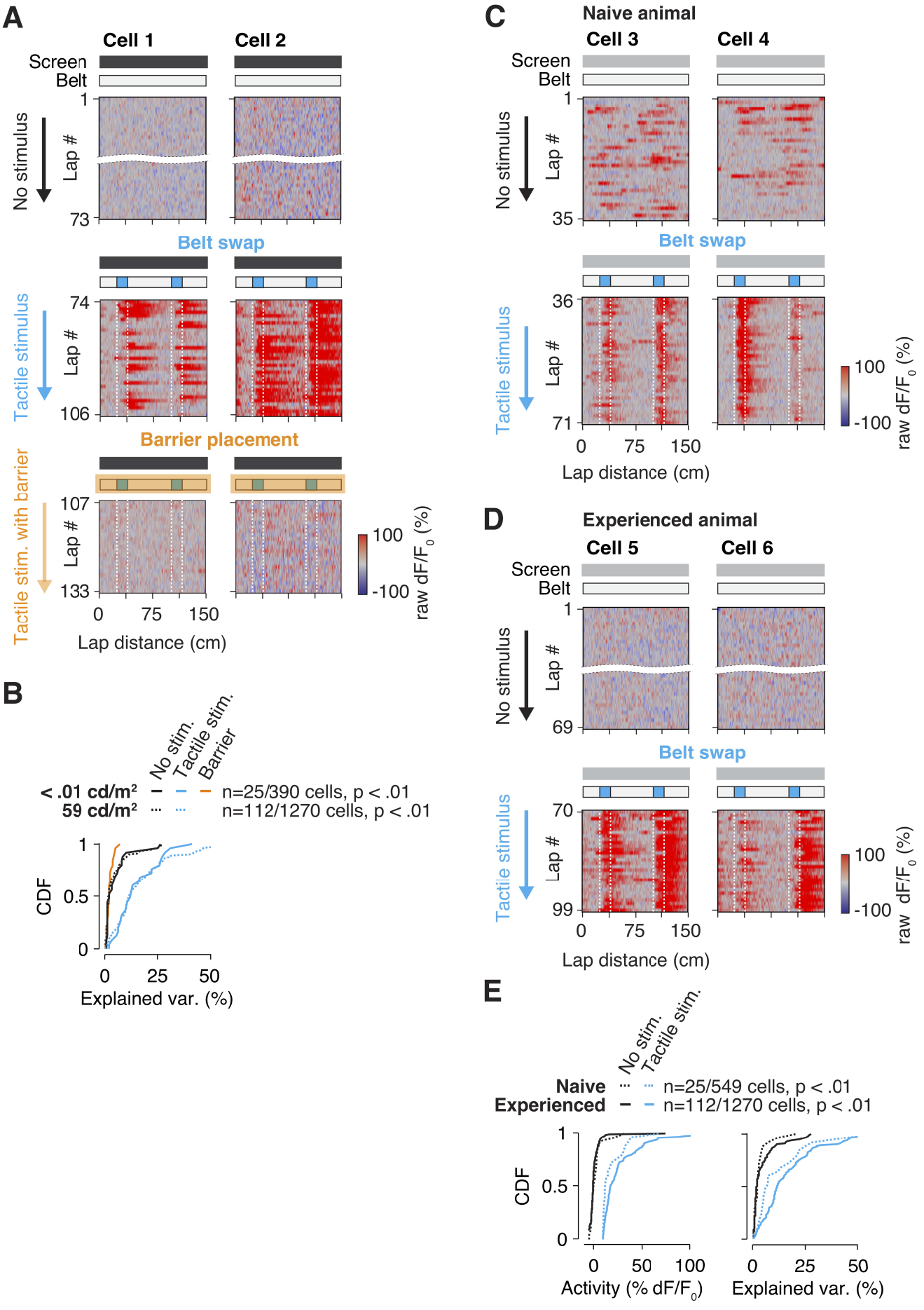

683 **Figure 3. Visual and Tactile Stimuli Activate Non-Overlapping V1 Populations**

684 Experiment demonstrating how visual and tactile stimuli activate distinct populations of V1
685 neurons.

686 (A) Trial average calcium fluorescence as a function of treadmill position of four V1 L2/3
687 neurons for a trial block on a treadmill without stimuli (left, n=24 laps), a block with unimodal
688 tactile stimulation (middle, n=23 laps), and a block with unimodal visual stimulation (right, n=17
689 laps). Tactile stimuli are as in Fig. 1. The visual stimulus is a 1-sec epoch of noise shown to the
690 right eye in a 60-by-60 deg. square window with onset triggered by treadmill locations. Cell
691 activated by tactile stimuli (cells 1,2) do not respond to visual stimulation, and vice versa (cells
692 3,4). See also Suppl. Figs S5, S6.

693 (B) Scatter plot shows visual vs. tactile responses for sensory responsive (n= 148, dark
694 markers) and nonresponsive (n = 568, grey markers) L2/3 neurons (1-way ANOVA, $p < 0.01$).
695 There is a complete dissociation by sensory modality. Visual activity is defined as calcium
696 activity in 1.5-sec windows after stimulus onset, tactile activity is defined as activity in 2-sec
697 windows after tactile stimuli.

698 (C) Scatter shows responses normalized to maximum response amplitude during either visual
699 or tactile stimulation.

700

Figure 3.

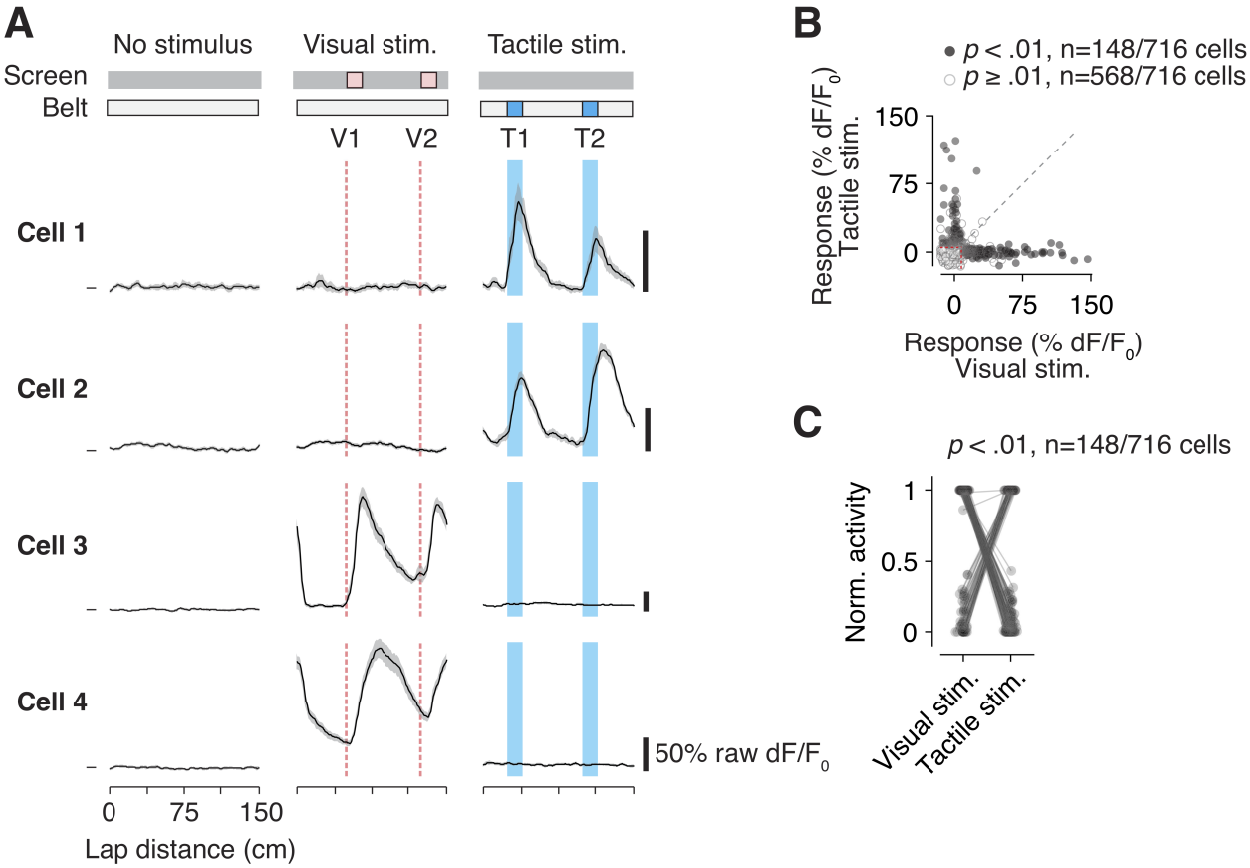

Figure 4. Diversity of Nonvisual V1 Activity in a Feature-Rich Tactile Environment

(A) Experiment to test for interactions between visual and tactile activity. A brief visual stimulus (top) is presented and diverse tactile stimuli of different heights and spatial configurations (middle and bottom) are placed at different locations on the treadmill.

(B,C) Example calcium time courses of ten simultaneously imaged V1 layer 2/3 neurons identified as visual (B, cells 1 to 4, red traces) or putative tactile (C, cells 5 to 10, blue traces) based on explained variance by position and visual stimulation (visual cells: EV visual stim. > 10 %; tactile cells: EV visual stim. ≤ 0 % and EV position > 10 %; see Experimental Procedures).

(D) Fraction of variance in calcium time courses explained by the visual stimulus. In contrast to visually neurons (n = 378 cells, red), other cells, including tactile activated neurons (n = 353 cells, blue), show no entrainment of activity by the visual stimulus (EV visual stim. ≤ 0 %). Red and blue markers indicate fraction of explained variance for example neurons in B,C.

(E) Fraction of variance in calcium activity explained by position for cells showing tactile activity (n = 353 cells; EV position > 10 %, EV visual stim. ≤ 0 %). Blue markers indicate fraction of explained variance for example neurons in C.

(F) Activity of visual neurons during still (dashed line) and running epochs (solid line). No visual stimulus is presented during stillness which leads to increased activity during running.

(G) Activity of putative tactile neurons during still (dashed line) and running epochs (solid line). Tactile neurons show similar activity during running and stillness, likely reflecting active whisking behaviour.

(H) Cumulative distribution of activity entrainment by treadmill position for cells imaged on the belt with diverse tactile stimuli (solid curve, see A), two stimuli (dashed curve, see Fig. 3) and without tactile stimuli (dotted curve, see Fig. 3). With diverse tactile stimuli, n = 686/1345 cells pass an EV threshold of 10 %, with two stimuli n = 144/716 cells, and without stimuli n = 38/716 cells. Dashed line indicates EV threshold.

Figure 4.

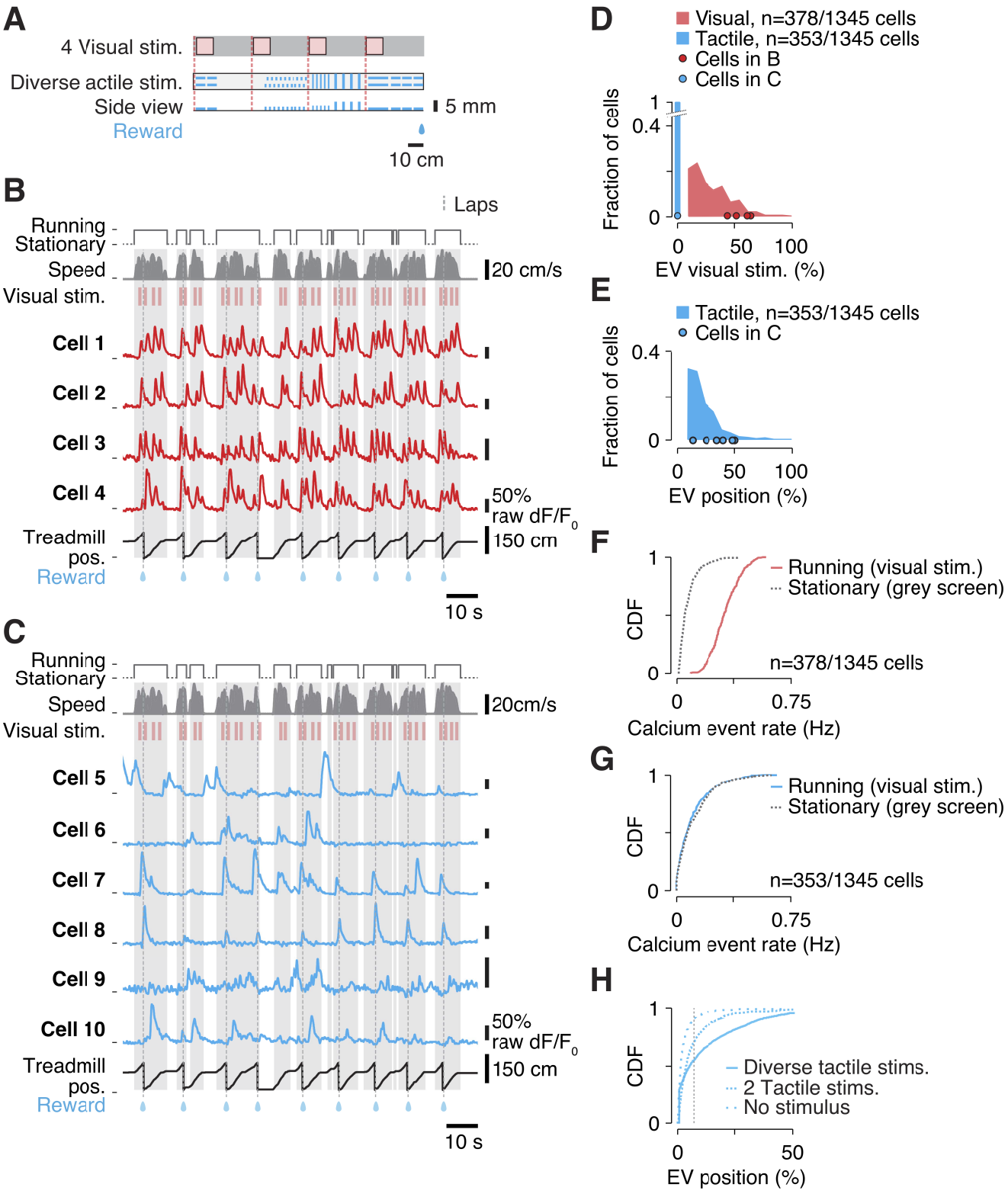

729 **Figure 5. V1 Tactile Activity is Diverse and Selective**

730 (A) Raster plots of calcium activity as a function of position of six simultaneously-imaged L2/3
731 neurons (cells 5 to 10 in Fig. 4C) on the treadmill with diverse tactile stimuli (top). The neurons
732 show diverse and selective activity. Dashed lines (red) indicate visual stimulus onset. For
733 contrasting visually evoked activity of cells 1 to 4 (Fig. 4) see raster plots in Suppl. Fig. S7.
734 (B) Trial average activity histogram of the activities in A.
735 (C) Auto-correlation half-width (correlation length) of position-related activity of the tactile V1
736 neurons. Blue markers indicate cells in A,B.
737 (D) Preferred position vs. selectivity index for neurons in C. Preferred position defined as belt
738 position of peak amplitude. Selectivity index defined as circular variance. Blue markers indicate
739 cells in A,B.
740 (E) Mean spatial population vector correlation matrix of the tactile V1 population activity. Note
741 how activity is clustered at specific belt positions visible in clustering of correlation coefficients.
742 See also Supp. Fig. S8.
743

Figure 5.

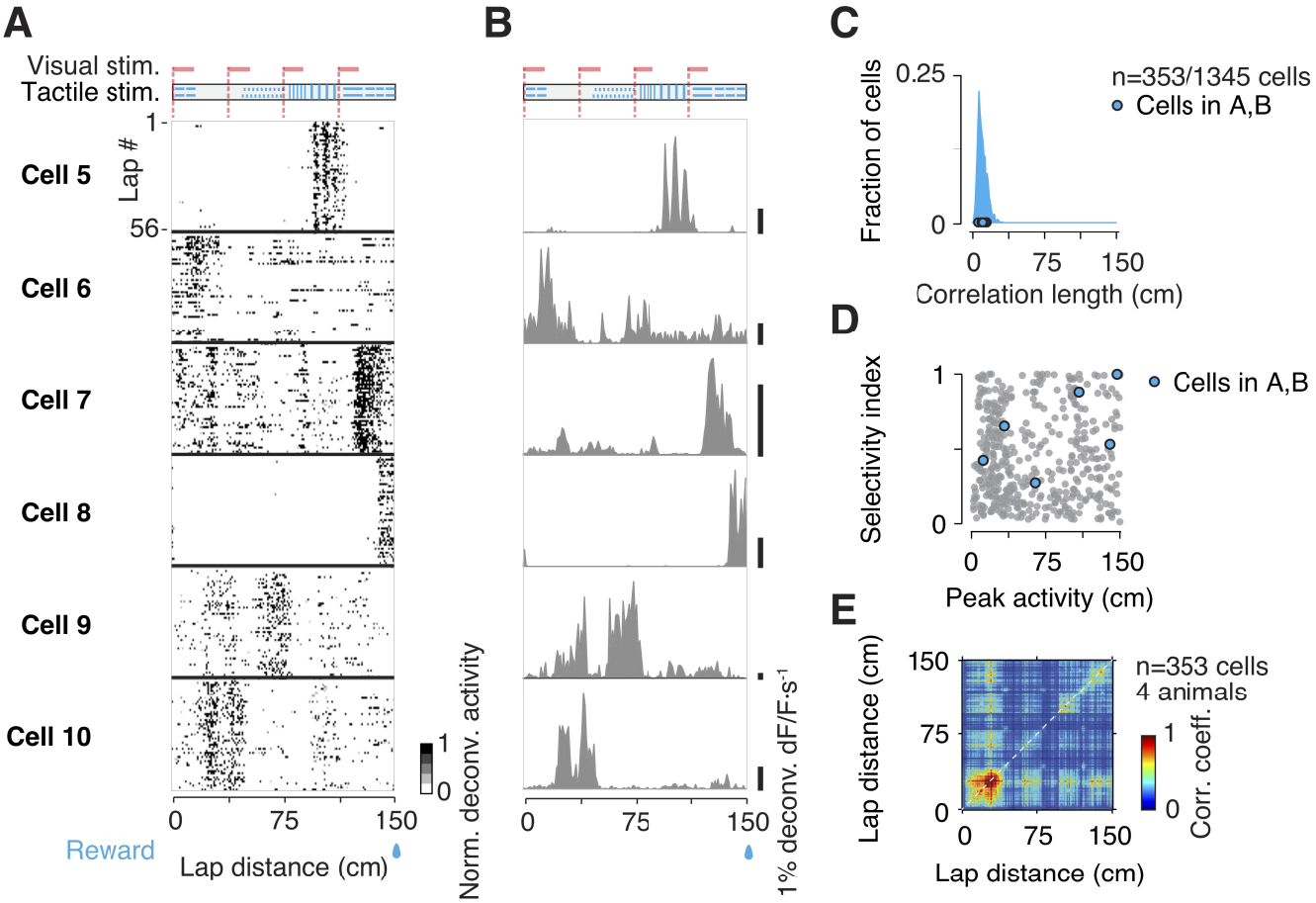

Figure 6. Evidence that Tactile Context Modulates V1 Visual Responses

(A) Visual response modulations. Top: The three visual stimulus windows A, B and C not accompanied by reward delivery are considered for investigating visual response modulations while the animal moves across locally distinct tactile stimuli (blue) on the belt. Bottom: Visual responses to identical noise stimulation of eight simultaneously imaged V1 cells while the animals move across treadmill positions A, B and C. Note how individual cells show distinct preferences to the stimuli presented at either treadmill position. Shaded curves represent s.e.m. MI indicates visual response modulation index. See also Suppl. Fig. S9A,B.

(B) Left: Average pupil dilation during visual stimulus windows A, B, C and R (reward). Right: Average locomotion speed during visual stimulus windows.

(C) Electrophysiology data. Histogram of response modulation index (MI) of the visually activated V1 population (all cells, grey; MI with effect size > 1, black). See also Suppl. Fig. S9A,B,D.

(D) Visual modulations extent across V1 layers. Left: Scatter of MI of electrophysiology data vs. cortical depth of recording site shows that visual response modulations. Right: Scatter of effect size (ES) vs. cortical depth. Black markers indicate MI with ES > 1.

(E) Same depiction as B for imaging data. See also Suppl. Fig. S9C.

(F) Visual response modulations depend on sensory information from tactile stimuli. Modulation index (left) and effect size (right) are decreased when contacts between whiskers and tactile stimuli are prevented (yellow curves).

Figure 6.

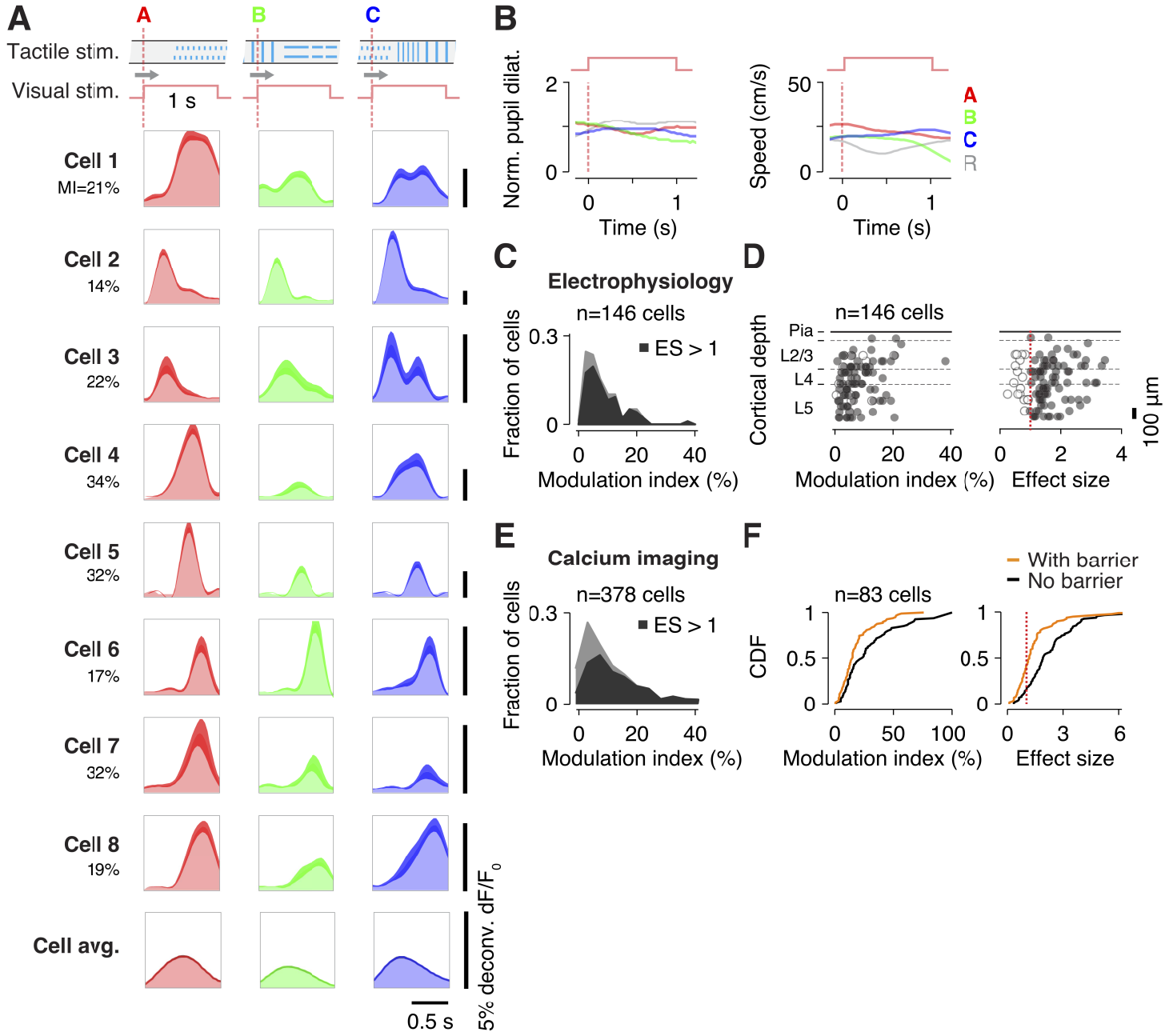

EXPERIMENTAL PROCEDURES

Animals

All animal procedures were approved by the Animal Ethics Committee of KU Leuven. We report on twenty-three normally-reared, single-housed male mice. Of these, nineteen were C57Bl/6j mice (22 to 30 gr, 2 to 5 months) and four were Thy1-GCaMP6 mice ((Dana et al., 2014). Mice were implanted with a head plate and trained to move on a linear, 150-cm treadmill belt for a periodic water reward (Royer et al., 2012). Eighteen mice were implanted with a cranial window for chronic cellular imaging (Goldey et al., 2014) in monocular V1 (n = 14), in CA1 pyramidal layer in dorsal hippocampus (n = 3 Thy1), or in S1 barrel cortex (n = 1 Thy1). Five mice were craniotomised for acute electrophysiological recordings with multi-site silicon probes.

Surgical Procedures

Mice were injected with dexamethasone (3.2 mg/kg I.M., 4 h before surgery), anesthetised with isoflurane (induced 3 %, 0.8 L/min O_2; sustained 1–1.5 %, 0.5 L/min O_2), and implanted with a titanium head plate.

For cellular imaging in V1 and S1, mice were craniotomised and implanted with a 5-mm cranial glass window centred over left visual cortex (1.6 mm anterior to lambda, 3.1 mm lateral to midline). Head plate and cranial windows were affixed with dental cement (Metabond, Crown & Bridge and Kerr Tab, Kerr Dental) mixed with black tempera pigment to provide light shielding during fluorescence imaging.

For cellular imaging in CA1, mice were craniotomised (2 mm anterior to lambda, 1.8 mm lateral to midline). A 3-mm-diameter slab of visual cortex above CA1 was ablated manually under visual guidance until cortical white matter was exposed. Mice were implanted with a 3-mm cranial window holding a 1.5-mm long glass tube, following surgical procedures as described.

For acute recordings, a 1-mm craniotomy was made above V1 (3.8 mm posterior to bregma, 2.5 mm lateral to midline). Two stainless steel screws used as reference and ground electrodes were implanted above cerebellum. Craniotomies were covered with a cover glass and protected with fast-curing silicone (Kwik-Cast, WPI).

All mice received post-operative treatment for 60 hours (buprenorphine 0.2 mg/kg I.M. and cefazolin 15 mg/kg I.M. in 12-hour intervals) and were given five days to recover.

Viral Vector Injections

Mice were injected with dexamethasone (3.2 mg/kg I.M., min. 4 h before surgery), anesthetized as described, and cranial windows were removed. An adeno-associated virus (AAV) construct containing GCaMP6m (n = 11 animals) or GCaMP6f (n = 3 animals) and the synapsin promotor (AAV1.Syn.GCaMP6m/f.WPRE.SV40, U Penn Vector Core) (Chen et al., 2013) was injected to monocular V1 or dorsal CA1. In V1, 500 nL AAV solution were injected at cortical depths of 250 to 450 μm. The AAV solution contained 25 % D-Mannitol solution (10 % in PBS) to increase transfection efficacy and 0.25 μL sulforhodamine SR101 for fluorescent monitoring of the loading (green light excitation, 560 nm; red light emission, 630 nm).
In CA1, 200 nL AAV solution were injected at depths of 1,500 μm before ablation of visual cortex (2 mm anterior to lambda, 1.8 mm lateral to midline).
Injections were performed using bevelled glass capillaries (~20 μm tip diameter, Drummond Sci.) at low injection rates (50 or 100 nL/min) using a microliter injection system (Nanoject II, Drummond Sci.). Cranial windows were replaced and mice recovered as described.

Treadmill Assay

The treadmill assay was adapted from Royer et al. (Royer et al., 2012) (Fig. 1A; Suppl. Fig. S1A). Two 3D-printed 10-cm diameter lightweight treadmill wheels mounted on a custom frame (Thorlabs) held a 150-cm long, 50-mm wide belt made of Velcro (Country Brook; experiments 1,2) or velvet fabric (McMaster-Carr; experiment 3) (Suppl. Fig. S2A–D). Strips of materials attached to the belt formed the tactile stimuli. The tactile stimuli were covered from the animals' eyesight by a shield mounted 10 to 15 mm in front of the animals' nose and 1 cm above the belt (–45 to 45 deg. azimuth, –30 deg. elevation) (Fig. 1A; Suppl. Fig. S1B,C). Teflon tape (CS Hyde) was adhered to the platform to reduce friction.
A rotary encoder (Avago Tech) attached to treadmill shaft was used to monitor treadmill rotation and belt position at a resolution of 3.14 mm. Once per treadmill rotation, for reward delivery, a photoelectric sensor (Omron) detected a reflective strip attached to the underside of the belt triggering opening of an electromagnetic pinch valve (MSscientific) and controlling water delivery through a spout. A custom circuit board with a microcontroller (AT89LP52, Atmel) monitored encoder and sensor signals and controlled valve opening. All signals were acquired by a personal computer via a USB data acquisition board (MCC) and were sampled at 10 kHz and recorded with Presentation software (Neurobehavioral Systems).

831

832 **Behavioural Training**

833 Mice were habituated to handling for three days prior to all procedures. Five days after surgery,
834 water intake was scheduled (1 mL per day), and animals were trained to head-fixed treadmill
835 locomotion on a copy of the experimental apparatus equipped with a belt without tactile stimuli
836 (Suppl. Fig. S2A). Mice were rewarded with tap water or 7.5 % sucrose solution, either manually
837 after habituation using a pipette or automated at the end of each lap (10 μL drop size). No visual
838 stimuli were presented during training (isoluminent grey screen or ambient illumination).
839 Training duration increased gradually from a few minutes to 1 hour per day over a period of two
840 weeks. Training was completed when animals reached desired levels of locomotor activity (~3
841 laps/min.).

842

843 **Flavoprotein Imaging**

844 Retinotopic mapping with flavoprotein imaging was used to determine the monocular subregion
845 of V1 that was targeted for chronic cellular imaging. Blue LED light (470 nm, Thorlabs) was
846 shone onto cortex and green light emission collected (510/84 nm filter, Semrock) at a frame rate
847 of 5 fps using a 2x wide-field lens (NA = 0.055, Edmund Optics) and EMCCD camera (EM-C^2,
848 QImaging; 1004 by 1002 pixels, 4 by 4 binning). Fractional changes in fluorescence were
849 normalised to baseline and averaged across 4-sec intervals to capture the slow time course of
850 the flavoprotein auto-fluorescence signal. The location of monocular V1 was identified by eye to
851 guide targeted viral vector delivery of the genetically encoded calcium indicator GCaMP6 at
852 retinotopic locations corresponding to monocular V1.

853

854 **Two-Photon Imaging**

855 A custom-built two-photon microscope (Neurolabware) was used to image somatic calcium
856 signals of V1 neurons in layer 2/3 (125 to 350 μm below the pial surface) and CA1 neurons in
857 dorsal hippocampus, pyramidal cell layer (100 to 150 μm below window) at frame rates of ~30
858 fps (1154 by 512 pixel, 620 by 380 μm field-of-view). Excitation light of a MaiTai DeepSee laser
859 with group-delay dispersion (Spectra Physics / Newport) was scanned by galvo (Cambridge
860 6215H) and resonant scanners (Cambridge CRS 8k) through a 16x lens (NA = 0.8, Nikon). Max.
861 laser power output at the objective was limited to 20 to 60 mW, depending on the depth of field-
862 of-view. GCaMP6 was excited at 920 nm and green light emission was collected using a green

filter (510/84 nm, Semrock) with a GaAsP photomultiplier tube (Hamamatsu). We used a black imaging chamber and blackout material (Thorlabs) to block stray light from the visual display (Goldey et al., 2014). Any leftover stray light (e.g. through the eyes and the brain) was subtracted out in the extraction of calcium time courses (Bonin et al., 2011).

Electrophysiology

A 256-channel DigiLynx system (Neuralynx) was used to record electrophysiological signals (sampling rate 32 kHz). A linear multi-site silicon probe (A16, 50 μm electrode spacing, NeuroNexus) was lowered perpendicularly into V1 at stereotactic coordinates (3.8 mm posterior to bregma, 2.5 mm lateral to midline) using a micromanipulator (Scientifica) at 10-μm steps. Once the probe penetrated the dura, the tip was lowered to cortical depths of 700 to 900 μm at 1-μm steps. The procedures were monitored with a surgical stereoscope. Recordings started 20 to 30 min after probes were in position and craniotomies were covered with 2.5 % agarose solution warmed to 37ºC. Silicon probes had impedances ranging from 1 to 2 MΩ.

Visual Stimulation

For visual stimulation, a calibrated 22-inch LCD monitor (Samsung 2233RZ, 1680 by 1050 pixel resolution, 60 Hz refresh rate, average luminance 59 cd/m^2) was positioned 18 cm in front of the right eye, covering 120 by 80 degree in the right visual field (0 to 120 deg. central to peripheral and ±40 deg. lower to upper visual field). Presentation software (Neurobehavioral Systems) was used to control visual stimulation, synchronised to the respective imaging frame rates of either one-photon (frame rate: 5 fps, EMCCD camera frame trigger) or two-photon (frame rate: ~30 fps, slow-axis galvanometer scan pulses) imaging. Visual stimulus frames were updated at 30 fps. Visual stimuli were interleaved by a static grey screen stimulus (50 % luminance).
For retinotopic mapping, six 8-sec stimuli were presented in the right visual field in 10 to 20 trials, covering a total of 0 to 120 deg. along the horizontal and ±40 deg. along the vertical axis. Stimuli were comprised of horizontally and vertically oriented, 40 by 40 deg. wide square-wave gratings moving in four cardinal directions (0.08 cpd spatial freq., 4 Hz temporal freq.). Stimuli were interleaved by a static, 16-sec grey screen stimulus.
For testing the visual responsiveness of V1 neurons, two sets of visual stimuli were presented: A brief, repeating 1-sec visual noise stimulus or prolonged, 7.8-sec filtered noise stimuli of broader visual stimulus space (Suppl. Fig. S6A). The brief noise stimulus was composed of

drifting oriented edges of different scales and orientations (Bonin et al., 2011) covering upper and lower sections of the right visual field (60 by 60 deg., centred at 45 deg. azimuth, 0 deg. elevation; Suppl. Fig. S1C). Stimulus presentation was triggered by the animals' movement across discrete belt positions. The prolonged stimuli were composed of filtered noise containing logarithmic increases in spatial frequency (0.05 to 0.4 cpd) in two temporal frequency bands (0.5 to 1 Hz and 1 to 2 Hz) and eight orientations (0 to 157.5 deg.) covering the full screen (120 by 80 deg.). Stimuli were interspersed by static, 50 % luminance grey screen stimuli.
For the experiment in darkness, ambient light sources were switched off or covered with blackout material. Light levels were at the detection threshold of our luminance meter (< 0.01 cd/m^2).

Eye Tracking

Eye position and pupil size were measured with an infrared eye tracking camera placed in front of the right eye. Infrared light was focused on the eye with a far-red LED (735 nm, Thorlabs) and collimated lens (Thorlabs). Data was acquired at 30 fps with a CCD camera (AVT Prosilica GC660; Navitar Zoom 6000 lens) and StreamPix software (Norpix) and segmented using custom software.

Experimental Design

Experiment 1: Mice (n = 7) first moved head-fixed on a treadmill belt without tactile stimuli for durations of 8 to 10 min. Subsequently, the belt was replaced with one containing two identical tactile stimuli at a distance from reward (Suppl. Fig. S2B) with the animals held in place maintaining the same imaging field-of-views. Tactile stimuli comprised four stereotyped foam material strips (2.5 cm spacing). The animals ran on the tactile belt for another 8 to 10 min. For a subset of animals (n = 4), experiments were performed in darkness in combination with a 3D-printed, removable barrier placed between the whiskers and the treadmill belt that prevented the whiskers from contacting the tactile stimuli. This approach was chosen over trimming the whiskers to avoid any form of plasticity that may occur upon whisker ablation. It was ensured the barrier did not contact the animal's nose or mouth to not impair receiving water reward or locomotion. The animals moved on the tactile belt with the barrier for another 8 to 10 min. An unconditional sucrose water reward (2.5 μL) was delivered in all conditions at the end of each lap.

Experiment 2: Mice (n = 7, same animals as in experiment 1) moved on a belt without tactile stimuli for 8 to 10 min. (Suppl. Fig. S2C). To elicit visual responses, the same 1-sec visual noise stimulus (Suppl. Fig. S1C; S2C,D) was triggered in every treadmill lap as the animals reached two discrete belt positions. Stimuli were interspersed by static grey screen stimuli of variable duration. The animals moved on the treadmill under visual stimulation for another 8 to 10 min. The belt was then replaced with the tactile belt described in experiment 1 and the animals moved for another 8 to 10 min.

To test visual responsiveness to a broader visual stimulus space, a separate group of animals (n = 3) moved on the treadmill with the prolonged filtered noise stimuli. Stimuli were presented for 7 to 10 trials and were not triggered by the animal's movement. Stimuli were interspersed by static grey screen stimuli of fixed duration (2 sec) (Suppl. Fig. S6A).

In both sets of runs, reward was delivered as described.

Experiment 3: A group of nine mice (4 used in V1 imaging, 5 in electrophysiology experiments) moved on a feature-rich tactile treadmill belt endowed with diverse tactile stimuli made from foam material, duct tape, and hot clue, attached to distinct belt positions (Suppl. Fig. S2D). The same brief visual noise stimulus was presented at four equidistant belt positions, thereby creating distinct combinations of the visual stimulus and varied tactile stimuli. Mice moved on the feature-rich belt for periods of 20 to 30 min. A group of three mice, moved on a feature-rich tactile belt in hippocampal imaging experiments without visual stimuli, in ambient light condition.

DATA ANALYSIS

All data were analysed in MATLAB (The Mathworks, Natick, MA).

Calcium Imaging Data

Images were registered using TurboReg (Thevenaz et al., 1998). Regions of interest (ROIs) of active neural cell bodies were identified manually using a pixelwise local spatiotemporal correlation criterion (3 by 3 pixels neighbourhood, thresholded at correlation coefficients > 0.95) (Smith and Hausser, 2010). Raw calcium time courses were calculated by averaging pixel intensities over each ROI and subtracting an estimate of neuropil contamination. The neuropil signal was computed by averaging a ring of pixels around ROIs and using a low-rank SVD approximation (Bonin et al., 2011). Raw calcium time courses were expressed as fractional changes above baseline fluorescence (dF/F_0). Baselines were computed by linear regression to

959 the lowest 10 % of the raw time courses. dF/F_0 time courses were deconvolved to estimate firing
960 rates (Vogelstein et al., 2010).
961
962 **Electrophysiology**
963 Raw voltage signals were high-pass filtered (0.8 to 5 kHz) for spike detection. All 16 channels
964 were grouped into four groups with each group containing four channels. Spike sorting was
965 done for each group. Spike waveforms were extracted, principal components computed and
966 automatically clustered with KlustaKwik (Kadir et al., 2014). Cluster quality was manually
967 verified or corrected using Klusters (Hazan et al., 2006). Only clusters with stable features
968 through time and clear refractory periods were included. We classified regular and fast spiking
969 neurons based on the peak-to-trough amplitude ratio and the end slope of their spike
970 waveforms (Niell and Stryker, 2008).
971
972 **Behavioural Data**
973 Rotary encoder increments were used to calculate treadmill position at centimetre precision and
974 instantaneous treadmill speed in cm/s. After every completed lap, encoder increments were
975 reset to zero to prevent potential accumulation of treadmill slip.
976 Camera frames from the eye tracker were smoothed with a 2D Gaussian filter, contrast-
977 thresholded, and binarised, resulting in black-and-white images. For every image, eye position
978 and pupil diameter were detected by fitting an ellipsis to the pupil. Pupil size was calculated
979 from the equivalent diameter of the ellipsis and expressed in mm^2. Eye position was expressed
980 as relative change in degree relative to the average eye centre position within individual
981 experiments. Artefacts in the data resulting from e.g. eye blinks were removed using a threshold
982 criterion (mean ± 2-times s.d.).
983 Encoder and eye data were resampled at the frame rate of the two-photon microscope.
984
985 **Selection of Active Neurons**
986 V1 neurons were selected if they exhibited one or more calcium transients in at least 25 % of
987 the laps (> baseline dF/F_0 + 3-times s.d.). This approach restricted analyses to neurons showing
988 a minimum of repeatable activation across laps.
989 CA1 neurons were selected if they exhibited position-normalized activity > .03 % dF/F_0 (see
990 Position Related Analysis).

991

992 **Visual Response Analysis**

993 Visual responsiveness (Fig. 4) was measured by computing the fraction of variance in the
994 calcium time courses that is explained by event-triggered averaged response models derived
995 from the neuron's deconvolved time courses at stimulus onsets (0 to 1 sec window) and offsets
996 (1 to 1.5 sec window), thereby including visual ON and OFF responsive cells. EV was two-fold
997 cross-validated (100-times) estimating how a random half of the trials predict the other half. EV
998 visual stim. is the sum of EVs calculated for stimulus onsets and offsets.

999

1000 **Position-Related Analysis**

1001 A standard position-related procedure was used to relate calcium time courses to location on
1002 the treadmill (Gothard et al., 1996). The treadmill lap was divided in 150 1-cm intervals for V1
1003 data and 100 1.5-cm intervals for CA1 data. Average deconvovled calcium activity was
1004 computed for each interval for each lap and normalized by the time the animal spent at each
1005 interval, resulting in position-related activity profiles. Accordingly, raw calcium time courses and
1006 locomotion speed were normalized to treadmill location with the same procedure (see Figs 1–3).
1007 Trial-to-trial reliability of activity profiles was measured by computing the fraction of variance in
1008 single trials that is explained by the average across laps. Formally, the measure of explained
1009 variance follows EV position = $(P_r–P_e)/P_r*100$, where P_r is the variance of the single trial
1010 responses and P_e is the mean square distance between single trial responses and the across
1011 trial. EV was two-fold cross-validated (100-times) estimating how a random half of the trials
1012 predicts the other half.

1013

1014 **Tactile Position Preference and Selectivity**

1015 A circular analysis was used to calculate for each tactile neuron the preferred belt position and
1016 position selectivity. Circular variance is commonly used to quantify tuning for circular variables
1017 (e.g. orientation selectivity). As the treadmill belt is circular this analysis is warranted here.
1018 Preferred position was determined by mapping the neurons' lap-to-lap activity average to a
1019 polar coordinate system with 1-cm intervals and calculating the angle of the vector sum of
1020 calcium activity. Position selectivity was defined as the circular variance of the polar
1021 representation of the average activity.

For each neuron, the auto-correlation of the position-normalized activity profiles was computed. The spatial extent of tactile activity was defined as the half-width of the auto-correlation function around zero lag at half-maximum amplitude.

Visual Response Modulations

For each visual neuron (EV visual stim. > 10 %), responses to the visual probe stimuli were sorted by onset location (Fig. 4A, Suppl. Fig. S9A). A modulation index (MI) was derived by projecting visual responses onto a polar 3-axes coordinate system (Suppl. Fig. S9B), with each axis shifted by 120 degrees and corresponding to one of the stimulus locations A to C. MI was computed by dividing the vector sum by the average response across stimuli, using the formula: $MI = [P_A+P_B+P_C]/\sum(P_i)*100$.

The effect size (ES), or d-prime – a measure quantifying differences in mean, of the response modulation was computed from the distributions of the data and a response shuffle across stimulus locations (Suppl. Fig. S9B).

MI and ES analyses were restricted to the stimuli triggered at track locations A, B and C to exclude potential bias from reward context (location R) (Suppl. Fig. S9A).

Correlation with Behavioural Variables

Spike responses of visual V1 neurons were correlated with behavioural variables locomotion speed (instantaneous speed at stimulus onset), eye position (relative position of pupil centre), and visual stimulation rate (stimulus frequency in the past 10 sec). Visual responses and behavioural variables were averaged within visual stimulus windows (0 to 1 sec after stimulus onset). Results were plotted in joint histograms with 10 equal-sized bins for the Pearson correlation coefficients between neural activity and behavioural variable, and 20 bins for the neuron's modulation indices (Suppl. Fig. S9E).

Joint histograms of modulation indices and effect sizes were generated for calcium imaging data for lap durations with the bottom and top 25 % of laps, averaged from a window centred around the reward location (-5 to 10 cm) (Suppl. Fig. S9F).

Population Vector Analysis

A standard spatial analysis was used to relate calcium activity to treadmill location (Terrazas et al., 2005). Mean population vector correlation matrices for CA1 and V1 data were computed from the averaged position-normalized activity profiles of individual neurons (Suppl. Fig. S8).